2. Spatial Pattern Formation with Reaction Diffusion Systems

2.1 Role of Pattern in Biology

Embryology is that part of biology which is concerned with the formation and development of the embryo from fertilization until birth. Development of the embryo is a sequential process and follows a ground plan, which is usually laid down very early in gestation. In humans, for example, it is set up roughly by the 5th week. There are many books on the subject; the one by Slack (1983) is a readable account of the early stages of development from egg to embryo. Morphogenesis, the part of embryology with which we are mainly concerned, is the development of pattern and form. How the developmental ground plan is established is unknown as are the mechanisms which produce the spatial patterning necessary for specifying the various organs.[1]

The following chapters and most of this one will be devoted to mechanisms which can generate spatial pattern and form, and which have been proposed as possible pattern formation processes in a variety of developmental situations. Wave phenomena create spatial patterns, of course, but these are spatio-temporal patterns. Here we shall be concerned with the formation of steady state spatially heterogeneous spatial patterns. In this chapter we introduce and analyse reaction diffusion pattern formation mechanisms mainly with developmental biology in mind. Section 2.7, however, is concerned with an ecological aspect of pattern formation, which suggests a possible strategy for pest control—the mathematical analysis is different but directly relevant to many embryological situations.

The questions we would like to answer, or, more realistically, get any enlightenment about, are legion. For example, are there any general patterning principles that are shared by bacteria, which can form complex patterns and wolf packs when they mark

[1] Professor Jean-Pierre Aubin in his book on *Mutational and Morphological Analysis* notes that the adjective *morphological* is due to Goethe (1749–1832). Goethe spent a lot of time thinking and writing about biology (the discipline 'biology' dates from 1802). Aubin goes on to describe Goethe's theory of plant evolution that hypothesizes that most plants come from one archetypal plant. Except for Geoffroy St. Hilaire, a distinguished early 19th century French biologist who wrote extensively about teratologies, or monsters (see Chapter 7), it was not taken seriously. Goethe was very bitter about it and complained about the difficulties in trying to work in a discipline other than one's own: it is still a problem. Goethe's work had some reevaluation in the 20th century, primarily by historians of science (see, for example, Lenoir 1984, Brady 1984 and other references there).

out territory? Spatial patterns are ubiquitous in the biomedical sciences and understanding how they are formed is without question one of the major fundamental scientific challenges. In the rest of the book we shall study a variety of pattern formation mechanisms which generate pattern in a variety of diverse areas.

Cell division starts after fertilisation. When sufficient cell division has taken place in a developing embryo the key problem is how the homogeneous mass of cells are spatially organised so that the sequential process of development can progress. Cells differentiate, in a biological sense, according to where they are in the spatial organisation. They also move around in the embryo. This latter phenomenon is an important element in morphogenesis and has given rise to a new approach to the generation of pattern and form discussed in some detail in Chapter 6.

It is impossible not to be fascinated and enthralled with the wealth, diversity and beauty of pattern in biology. Figure 2.1 shows only four examples. How such patterns, and millions of others, were laid down is still unknown although considerable progress has been made in several different fronts such as in the early patterning in the embryo of the fruit fly, spatial patterning in slime moulds and bacterial patterns discussed in Chapter 5. The patterning problems posed by only the few patterns in Figure 2.1 are quite diverse.

As a footnote to Figure 2.1(c), note the antennae on the moth. These antennae very effectively collect molecules of the chemical odorant, called a pheromone called bombykol, which is exuded by the female to attract the male. In the case of the silk moth the male, which cannot fly, can detect the pheromone from the female as far away as a kilometre and can move up the concentration gradient towards the female. The filtering efficiency of such antennae, which collect, and in effect count, the molecules, poses a very different and interesting mathematical biology patterning problem to those discussed in this book, namely, how such a filter antenna should be designed to be most efficient. This specific problem—an interesting fluid mechanics and diffusion one—was discussed in detail by Murray (1977).

The fundamental importance of pattern and form in biology is self-evident. Our understanding is such that whatever pattern we observe in the animal world, it is almost certain that the process that produced it is still unknown. Pattern formation studies have often been criticized for their lack of inclusion of genes in the models. But then the criticism can be levelled at any modelling abstraction of a complex system to a relatively simple one. It should be remembered that the generation of pattern and form, particularly in development, is usually a long way from the level of the genome. Of course genes play crucial roles and the mechanisms must be genetically controlled; the genes, however, themselves cannot create the pattern. They only provide a blueprint or recipe, for the pattern generation. Many of the evolving patterns could hardly have been anticipated solely by genetic information. Another of the major problems in biology is how genetic information is physically translated into the necessary pattern and form. Much of the research in developmental biology, both experimental and theoretical, is devoted to trying to determine the underlying mechanisms which generate pattern and form in early development. The detailed discussion in these next few chapters discusses some of the mechanisms which have been proposed and gives an indication of the role of mathematical modelling in trying to unravel the underlying mechanisms involved in morphogenesis.

(a)

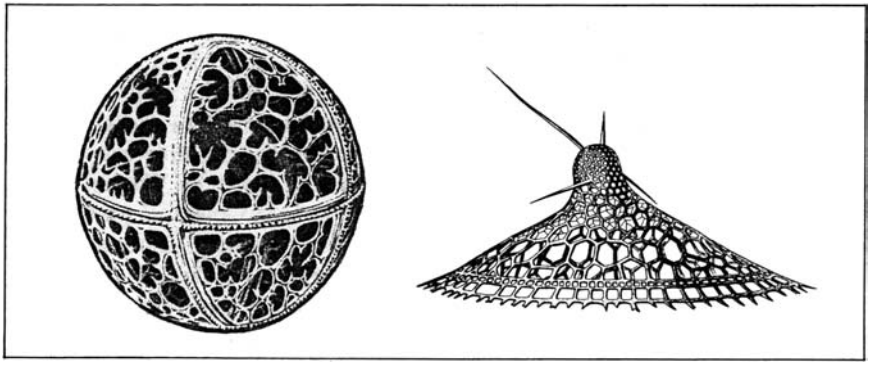

(b)

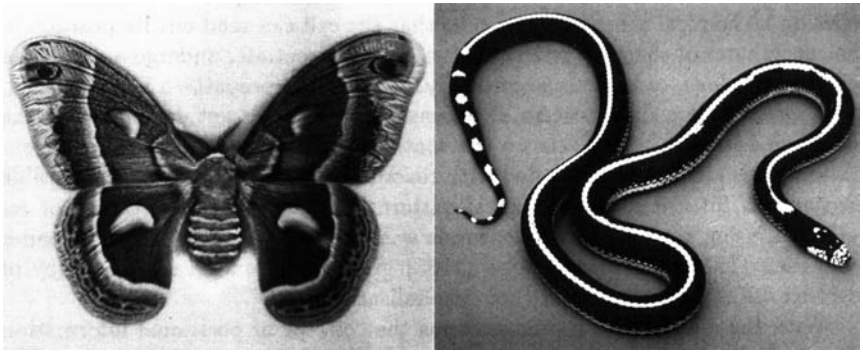

(c) (d)

Figure 2.1. (**a**) Leopard (*Panthera pardus*) in the Serengeti National Park, Tanzania. Note the individual spot structure. (Photograph courtesy of Hans Kruuk) (**b**) Radiolarians (*Trissocyclus spaeridium* and *Eucecryphalus genbouri*). These are small marine organisms—protozoa—of the order of a millimeter across. (After Haekel 1862, 1887) The structural architecture of radiolarians is amazingly diverse (see, for example, the plate reproductions of some of Haeckel's drawings in the Dover Archive Series, Haeckel 1974, but see also the historical aside on Haeckel in Section 6.1). (**c**) Moth (*Hyalophora cecropia*). As well as the wing patterns note the stripe pattern on the body and the structure of the antennae. (**d**) California king snake. Sometimes the pattern consists of crossbands rather than a backstripe. (Photograph courtesy of Lloyd Lemke)

A phenomenological concept of pattern formation and differentiation called *positional information* was proposed by Wolpert (1969, see the reviews in 1971, 1981). He suggested that cells are preprogrammed to react to a chemical (or morphogen) concentration and differentiate accordingly, into different kinds of cells such as cartilage cells. The general introductory paper by Wolpert (1977) gives a very clear and nontechnical description of development of pattern and form in animals and the concepts and application of his positional information scenario. Although it is a phenomenological approach, with no actual mechanism involved it has given rise to an immense number of illuminating experimental studies, many associated with the development of the limb cartilage patterning in chick embryos and feather patterns on other bird embryos, such as the quail and guinea fowl (see, for example, Richardson et al. 1991 and references there). A literature search of positional information in development will produce an enormous number of references. Although it is a simple and attractive concept, which has resulted in significant advances in our knowledge of certain aspects of development, it is not a mechanism.

The chemical prepattern viewpoint of embryogenesis separates the process of development into several steps; the essential first step is the creation of a morphogen concentration spatial pattern. The name 'morphogen' is used for such a chemical because it effects morphogenesis. The notion of positional information relies on a chemical pre-specification so that the cell can read out its position in the coordinates of chemical concentration, and differentiate, undergo appropriate cell shape change, or migrate accordingly. So, once the prepattern is established, morphogenesis is a slave process. Positional information is not dependent on the specific mechanism which sets up the spatial prepattern of morphogen concentration. This chapter is concerned with reaction diffusion models as the possible mechanisms for generating biological pattern. The basic chemical theory or reaction diffusion theory of morphogenesis was put forward in the classical paper by Turing (1952). Reaction diffusion theory, which now has a vast literature, is a field of research in its own right.

With the complexity of animal forms the concept of positional information necessarily implies a very sophisticated interpretation of the 'morphogen map' by the cell. This need not pose any problem when we recall how immensely complex a cell is whether or not it is positional information or simply a cell responding in some way to small differences in chemical concentration. The scale of pattern that can be formed by reaction diffusion can be very small as seen in the experimental patterns shown in Figure 2.11. A very rough idea of cell complexity is given by comparing the weight per bit of information of the cell's DNA molecule (deoxyribonucleic acid) of around 10^{-22}, to that of, say, imaging by an electron beam of around 10^{-10} or of a magnetic tape of about 10^{-5}. The most sophisticated and compact computer chip is simply not in the same class as a cell.

An important point arising from theoretical models is that any pattern contains its own history. Consider the following simple engineering analogy (Murray et al. 1998) of our role in trying to understand a biological process. It is one thing to suggest that a bridge requires a thousand tons of steel, that any less will result in too weak a structure, and any more will result in excessive rigidity. It is quite another matter to instruct the workers on how best to put the pieces together. In morphogenesis, for example, it is conceivable that the cells involved in tissue formation and deformation have enough

expertise that given the right set of ingredients and initial instructions they could be persuaded to construct whatever element one wants. This is the hope of many who are searching for a full and predictive understanding. However, it seems very likely that the global effect of all this sophisticated cellular activity would be critically sensitive to the sequence of events occurring during development. As scientists we should concern ourselves with how to take advantage of the limited opportunities we have for communicating with the workforce so as to direct experiment towards an acceptable end-product.

None of the individual models that have been suggested for any biological patterning process, and not even all of them put together, could be considered a complete model. In the case of some of the widely studied problems (such as patterning in the developing limb bud), each model has shed light on different aspects of the process and we can now say what the important conceptual elements have to be in a complete model. These studies have served to highlight where our knowledge is deficient and to suggest directions in which fruitful experimentation might lead us. Indeed, a critical test of these theoretical constructs is in their impact on the experimental community.[2]

To conclude this section it must be stressed again that mathematical descriptions, including phenomenological descriptions, of patterning scenarios are *not* explanations. This is generally accepted, but often forgotten.

2.2 Reaction Diffusion (Turing) Mechanisms

Turing (1952) suggested that, under certain conditions, chemicals can react and diffuse in such a way as to produce steady state heterogeneous spatial patterns of chemical or morphogen concentration. In Chapter 11, Volume I we derived the governing equations for reaction diffusion mechanisms, namely, (11.16), which we consider here in the form:

$$\frac{\partial \mathbf{c}}{\partial t} = \mathbf{f}(\mathbf{c}) + D\nabla^2\mathbf{c}, \tag{2.1}$$

where $\mathbf{c}$ is the vector of morphogen concentrations, $\mathbf{f}$ represents the reaction kinetics and D is the diagonal matrix of positive constant diffusion coefficients. This chapter is mainly concerned with models for two chemical species, $A(\mathbf{r}, t)$ and $B(\mathbf{r}, t)$ say. The equation system is then of the form

$$\begin{aligned} \frac{\partial A}{\partial t} &= F(A, B) + D_A\nabla^2 A, \\ \frac{\partial B}{\partial t} &= G(A, B) + D_B\nabla^2 B, \end{aligned} \tag{2.2}$$

where F and G are the kinetics, which will always be nonlinear.

[2] In the case of the mechanical theory of pattern formation discussed later, after some discussion, Lewis Wolpert (a friend and colleague of many years) who did not believe in the mechanical theory of pattern formation, designed some experiments specifically to disprove the theory. Although the experiments did not in fact do so, he discovered something else about the biological process he was studying—patterning in the chick limb bud. The impact of the theory was biologically illuminating even if the motivation was not verification. As he freely admits, he would not have done these specific experiments had he not been stimulated (or rather provoked) to do so by the theory.

Turing's (1952) idea is a simple but profound one. He said that, if in the absence of diffusion (effectively $D_A = D_B = 0$), A and B tend to a linearly stable uniform steady state then, under certain conditions, which we shall derive, spatially inhomogeneous patterns can evolve by *diffusion driven instability* if $D_A \neq D_B$. Diffusion is usually considered a *stabilising* process which is why this was such a novel concept. To see intuitively how diffusion can be destablising consider the following, albeit unrealistic, but informative analogy.

Consider a field of dry grass in which there is a large number of grasshoppers which can generate a lot of moisture by sweating if they get warm. Now suppose the grass is set alight at some point and a flame front starts to propagate. We can think of the grasshopper as an inhibitor and the fire as an activator. If there were no moisture to quench the flames the fire would simply spread over the whole field which would result in a uniform charred area. Suppose, however, that when the grasshoppers get warm enough they can generate enough moisture to dampen the grass so that when the flames reach such a pre-moistened area the grass will not burn. The scenario for spatial pattern is then as follows. The fire starts to spread—it is one of the 'reactants,' the activator, with a 'diffusion' coefficient D_F say. When the grasshoppers, the inhibitor 'reactant,' ahead of the flame front feel it coming they move quickly well ahead of it; that is, they have a 'diffusion' coefficient, D_G say, which is much larger than D_F. The grasshoppers then sweat profusely and generate enough moisture to prevent the fire spreading into the moistened area. In this way the charred area is restricted to a finite domain which depends on the 'diffusion' coefficients of the reactants—fire and grasshoppers—and various 'reaction' parameters. If, instead of a single initial fire, there were a random scattering of them we can see how this process would result in a final spatially heterogeneous steady state distribution of charred and uncharred regions in the field and a spatial distribution of grasshoppers, since around each fire the above scenario would take place. If the grasshoppers and flame front 'diffused' at the same speed no such spatial pattern could evolve. It is clear how to construct other analogies; other examples are given below in Section 2.3 and another in the *Scientific American* article by Murray (1988).

In the following section we describe the process in terms of reacting and diffusing morphogens and derive the necessary conditions on the reaction kinetics and diffusion coefficients. We also derive the type of spatial patterns we might expect. Here we briefly record for subsequent use two particularly simple hypothetical systems and one experimentally realised example, which are capable of satisfying Turing's conditions for a pattern formation system. There are now many other systems which have been used in studies of spatial patterning. These have varying degrees of experimental plausibility. With the extensive discussion of the Belousov–Zhabotinskii reaction in Chapter 8, Volume I and the last chapter we should particularly note it. Even though many other real reaction systems have been found it is still the major experimental system.

The simplest system is the Schnakenberg (1979) reaction discussed in Chapter 7, Volume I which, with reference to the system form (2.2), has kinetics

$$\begin{aligned} F(A, B) &= k_1 - k_2 A + k_3 A^2 B, \\ G(A, B) &= k_4 - k_3 A^2 B, \end{aligned} \tag{2.3}$$

where the k's are the positive rate constants. Here A is created autocatalytically by the k_3A^2B term in $F(A, B)$. This is one of the prototype reaction diffusion systems. Another is the influential activator–inhibitor mechanism suggested by Gierer and Meinhardt (1972) and widely studied and used since then. Their system was discussed in Chapter 6, Volume I and is

$$F(A, B) = k_1 - k_2A + \frac{k_3A^2}{B}, \quad G(A, B) = k_4A^2 - k_5B, \tag{2.4}$$

where here A is the activator and B the inhibitor. The k_3A^2/B term is again autocatalytic. Koch and Meinhardt (1994) review the applications of the Gierer–Meinhardt reaction diffusion system to biological pattern formation of complex structures. They give an extensive bibliography of applications of this specific model and its variations.

The real empirical substrate-inhibition system studied experimentally by Thomas (1975) and also described in detail in Chapter 6, Volume I, has

$$\begin{aligned} &F(A, B) = k_1 - k_2A - H(A, B), \quad G(A, B) = k_3 - k_4B - H(A, B), \\ &H(A, B) = \frac{k_5AB}{k_6 + k_7A + k_8A^2}. \end{aligned} \tag{2.5}$$

Here A and B are respectively the concentrations of the substrate oxygen and the enzyme uricase. The substrate inhibition is evident in the H-term via k_8A^2. Since the H-terms are negative they contribute to reducing A and B; the rate of reduction is inhibited for large enough A. Reaction diffusion systems based on the Field–Körös–Noyes (FKN) model kinetics (cf. Chapter 8, Volume I) is a particularly important example because of its potential for experimental verification of the theory; references are given at the appropriate places below.

Before commenting on the types of reaction kinetics capable of generating pattern we must nondimensionalise the systems given by (2.2) with reaction kinetics from such as (2.3) to (2.5). By way of example we carry out the details here for (2.2) with F and G given by (2.3) because of its algebraic simplicity and our detailed analysis of it in Chapter 7, Volume I. Introduce L as a typical length scale and set

$$\begin{aligned} &u = A\left(\frac{k_3}{k_2}\right)^{1/2}, \quad v = B\left(\frac{k_3}{k_2}\right)^{1/2}, \quad t^* = \frac{D_At}{L^2}, \quad \mathbf{x}^* = \frac{\mathbf{x}}{L}, \\ &d = \frac{D_B}{D_A}, \quad a = \frac{k_1}{k_2}\left(\frac{k_3}{k_2}\right)^{1/2}, \quad b = \frac{k_4}{k_2}\left(\frac{k_3}{k_2}\right)^{1/2}, \quad \gamma = \frac{L^2k_2}{D_A}. \end{aligned} \tag{2.6}$$

The dimensionless reaction diffusion system becomes, on dropping the asterisks for algebraic convenience,

$$\begin{aligned} u_t &= \gamma(a - u + u^2v) + \nabla^2u = \gamma f(u, v) + \nabla^2u, \\ v_t &= \gamma(b - u^2v) + d\nabla^2v = \gamma g(u, v) + d\nabla^2v, \end{aligned} \tag{2.7}$$

where f and g are defined by these equations. We could incorporate γ into new length and timescales by setting $\gamma^{1/2}\mathbf{r}$ and γt for $\mathbf{r}$ and t respectively. This is equivalent to defining the length scale L such that $\gamma = 1$; that is, $L = (D_A/k_2)^{1/2}$. We retain the specific form (2.7) for reasons which become clear shortly as well as for the analysis in the next section and for the applications in the following chapters.

An appropriate nondimensionalisation of the reaction kinetics (2.4) and (2.5) give (see Exercise 1)

$$\begin{aligned} &f(u,v) = a - bu + \frac{u^2}{v}, \quad g(u,v) = u^2 - v, \\ &f(u,v) = a - u - h(u,v), \quad g(u,v) = \alpha(b-v) - h(u,v), \\ &h(u,v) = \frac{\rho u v}{1 + u + Ku^2}, \end{aligned} \tag{2.8}$$

where a, b, α, ρ and K are positive parameters. If we include activator inhibition in the activator–inhibitor system in the first of these we have, for f and g,

$$f(u,v) = a - bu + \frac{u^2}{v(1+ku^2)}, \quad g(u,v) = u^2 - v, \tag{2.9}$$

where k is a measure of the inhibition; see also Section 6.7 in Chapter 6 in Volume I. Murray (1982) discussed each of these systems in detail and drew conclusions as to their relative merits as pattern generators; he presented a systematic analytical method for studying any two-species reaction diffusion system. For most pattern formation (analytical) illustrations with reaction diffusion mechanisms the simplest, namely, (2.7), turned out to be the most robust of those considered and, fortunately, the easiest to study.

All such reaction diffusion systems can be nondimensionalised and scaled to take the general form

$$u_t = \gamma f(u,v) + \nabla^2 u, \quad v_t = \gamma g(u,v) + d\nabla^2 v, \tag{2.10}$$

where d is the ratio of diffusion coefficients and γ can have any of the following interpretations.

(i) $\gamma^{1/2}$ is proportional to the *linear* size of the spatial domain in one dimension. In two dimensions γ is proportional to the area. This meaning is particularly important as we shall see later in Section 2.5 and in Chapter 3.

(ii) γ represents the relative strength of the reaction terms. This means, for example, that an increase in γ may represent an increase in activity of some rate-limiting step in the reaction sequence.

(iii) An increase in γ can also be thought of as equivalent to a decrease in the diffusion coefficient ratio d.

Particular advantages of this general form are: (a) the dimensionless parameters γ and d admit a wider biological interpretation than do the dimensional parameters and (b) when we consider the domains in parameter space where particular spatial patterns appear, the results can be conveniently displayed in (γ, d) space. This aspect was exploited by Arcuri and Murray (1986).

Whether or not the systems (2.2) are capable of generating Turing-type spatial patterns crucially depends on the reaction kinetics f and g, and the values of γ and d. The detailed form of the null clines provides essential initial information. Figure 2.2 illustrates typical null clines for f and g defined by (2.7)–(2.9).

In spite of their different chemical motivation and derivation all of these kinetics are equivalent to some activation–inhibition interpretation and when coupled with unequal diffusion of the reactants, are capable of generating spatial patterns. The spatial activation–inhibition concept was discussed in detail in Section 11.5 in Chapter 11 in Volume I, and arose from an integral equation formulation: refer to equation (11.41) there. As we shall see in the next section the crucial aspect of the kinetics regarding pattern generation is incorporated in the form of the null clines and how they intersect in the vicinity of the steady state. There are two broad types illustrated in the last fig-

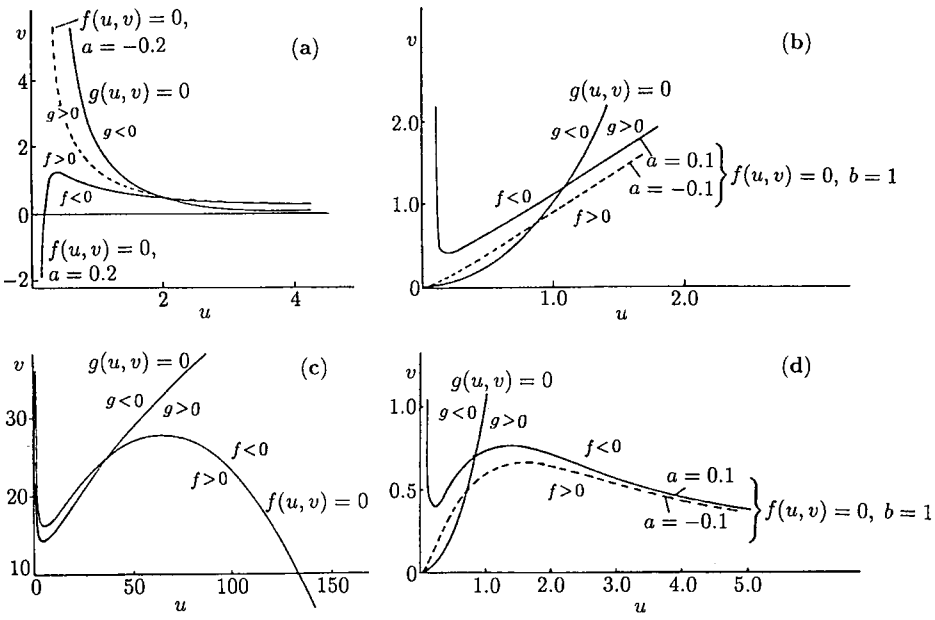

Figure 2.2. Null clines $f(u, v) = 0$, $g(u, v) = 0$: (**a**) The dimensionless Schnakenberg (1979) kinetics (2.7) with $a = 0.2$ and $b = 2.0$ with the dashed curve, where $a = -0.2$ and which is typical of the situation when $a < 0$. (**b**) The dimensionless Gierer and Meinhardt (1972) system with $a = \pm 0.1$, $b = 1$ and no activator inhibition. (**c**) The empirical Thomas (1975) system defined by (2.8) with parameter values $a = 150$, $b = 100$, $\alpha = 1.5$, $\rho = 13$, $K = 0.05$. (**d**) The kinetics in (2.9) with $a > 0$, $b > 0$ and $k > 0$, which implies activator inhibition; the dashed curve has $a < 0$.

ure. The steady state neighbourhood of the null clines in Figures 2.2(b), (c) and (d) are similar and represent one class, while that in Figure 2.2(a) is the other.

We should note here that there are other important classes of null clines which we do not consider, such as those in which there is more than one positive steady state; we discussed such kinetics in Chapter 7, Volume I for example. Reaction diffusion systems with such kinetics can generate even more complex spatial patterns: initial conditions here are particularly important. We also do not discuss here systems in which the diffusion coefficients are space-dependent and concentration- or population-dependent; these are important in ecological contexts (recall the discussion in Chapter 1 on the spread of genetically engineered organisms). We briefly considered density-dependent diffusion cases in Chapter 11, Volume I. Later in the book we discuss an important application in which the diffusion coefficient is space-dependent when we model the spread of brain tumours in anatomically realistic brains.

It is often useful and intuitively helpful in model building to express the mechanism's kinetics in schematic terms with some convention to indicate autocatalysis, activation, inhibition, degradation and unequal diffusion. If we do this, by way of illustration, with the activator–inhibitor kinetics given by the first of (2.8) in (2.10) we can adopt the convention shown in Figure 2.3(a).

The effect of different diffusion coefficients, here with $d > 1$, is to illustrate the prototype spatial concept of local activation and lateral inhibition illustrated in Figures 2.3(b) and 2.4(b). The general concept was introduced before in Chapter 11, Volume I. It is this generic spatial behaviour which is necessary for spatial patterning: the grasshoppers and the fire analogy is an obvious example with the fire the local activation and the grasshoppers providing the long range inhibition. It is intuitively clear that the diffusion coefficient of the inhibitor must be larger than that of the activator.

The concept of local activation and lateral inhibition is quite old going back at least to Ernst Mach in 1885 with his Mach bands. This is a visual illusion which occurs when dark and light bands are juxtaposed. Figure 2.4 is a schematic illustration of what happens together with an example of the Hermann illusion which is based on it.

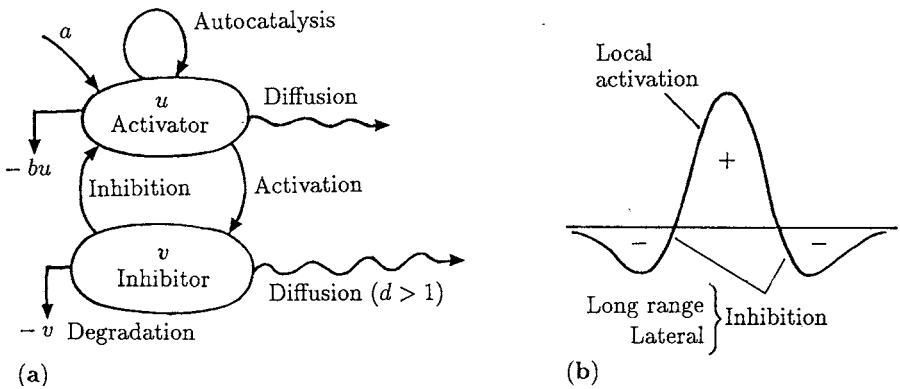

Figure 2.3. (**a**) Schematic representation of the activator–inhibitor system $u_t = a - bu + (u^2/v) + \nabla^2 u$, $v_t = u^2 - v + d\nabla^2 v$. (**b**) Spatial representation of local activation and long range inhibition.

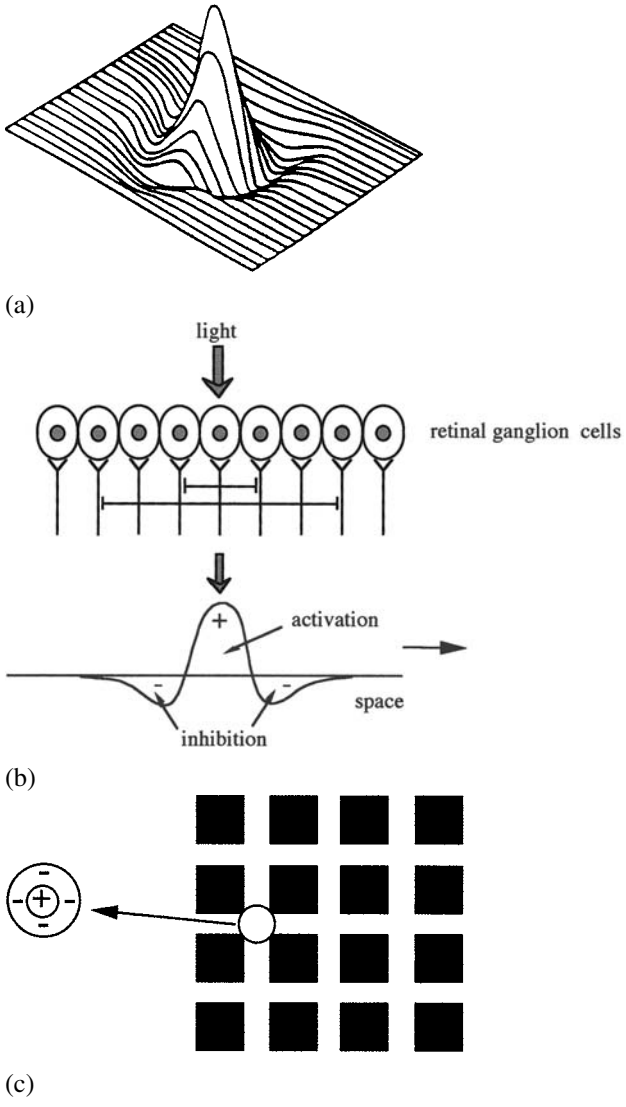

Figure 2.4. (**a**) If a light is shone on an array of retinal ganglion cells there is local activation of the cells in the immediate neighbourhood of the light with lateral inhibition of the cells farther away from the light source. The result is a landscape of local activation and lateral inhibition as illustrated in (**b**). (**c**) This illustrates the Hermann illusion. Here cells have more illumination in their inhibitory surrounding regions than cells in other white regions and so are more strongly inhibited and appear darker.

2.3 General Conditions for Diffusion-Driven Instability: Linear Stability Analysis and Evolution of Spatial Pattern

A reaction diffusion system exhibits diffusion-driven instability, sometimes called Turing instability, if the homogeneous steady state is stable to small perturbations in the absence of diffusion but unstable to small *spatial* perturbations when diffusion is present. The concept of instability in biology is often in the context of ecology, where a uniform steady state becomes unstable to small perturbations and the populations typically exhibit some temporal oscillatory behaviour. The instability we are concerned with here is of a quite different kind. The main process driving the spatially inhomogeneous instability is diffusion: the mechanism determines the spatial pattern that evolves. How the pattern or mode is selected is an important aspect of the analysis, a topic we discuss in this (and later) chapters.

We derive here the necessary and sufficient conditions for diffusion-driven instability of the steady state and the initiation of spatial pattern for the general system (2.10). To formulate the problem mathematically we require boundary and initial conditions. These we take to be zero flux boundary conditions and given initial conditions. The mathematical problem is then defined by

$$\begin{aligned} &u_t = \gamma f(u,v) + \nabla^2 u, \quad v_t = \gamma g(u,v) + d\nabla^2 v, \\ &(\mathbf{n}\cdot\nabla)\begin{pmatrix} u \\ v \end{pmatrix} = 0, \quad \mathbf{r} \text{ on } \partial B; \quad u(\mathbf{r},0),\ v(\mathbf{r},0) \text{ given}, \end{aligned} \tag{2.11}$$

where ∂B is the closed boundary of the reaction diffusion domain B and $\mathbf{n}$ is the unit outward normal to ∂B. There are several reasons for choosing zero flux boundary conditions. The major one is that we are interested in self-organisation of pattern; zero flux conditions imply no external input. If we imposed fixed boundary conditions on u and v the spatial patterning could be a direct consequence of the boundary conditions as we shall see in the ecological problem below in Section 2.7. In Section 2.4 we carry out the analysis for a specific one- and two-dimensional situation with the kinetics given by (2.7).

The relevant homogeneous steady state (u_0, v_0) of (2.11) is the positive solution of

$$f(u,v) = 0, \quad g(u,v) = 0. \tag{2.12}$$

Since we are concerned with *diffusion-driven* instability we are interested in linear instability of this steady state that is solely *spatially* dependent. So, in the absence of any spatial variation the homogeneous steady state must be linearly stable: we first determine the conditions for this to hold. These were derived in Chapter 3, Volume I but as a reminder and for notational completeness we briefly rederive them here.

With no spatial variation u and v satisfy

$$u_t = \gamma f(u,v), \quad v_t = \gamma g(u,v). \tag{2.13}$$

Linearising about the steady state (u_0, v_0) in exactly the same way as we did in Chapter 3, Volume I, we set

$$\mathbf{w} = \begin{pmatrix} u - u_0 \\ v - v_0 \end{pmatrix} \tag{2.14}$$

and (2.13) becomes, for $|\,\mathbf{w}\,|$ small,

$$\mathbf{w}_t = \gamma A\mathbf{w}, \quad A = \begin{pmatrix} f_u & f_v \\ g_u & g_v \end{pmatrix}_{u_0, v_0}, \tag{2.15}$$

where A is the stability matrix. From now on we take the partial derivatives of f and g to be evaluated at the steady state unless stated otherwise. We now look for solutions in the form

$$\mathbf{w} \propto e^{\lambda t}, \tag{2.16}$$

where λ is the eigenvalue. The steady state $\mathbf{w} = 0$ is linearly stable if $\mathrm{Re}\,\lambda < 0$ since in this case the perturbation $\mathbf{w} \to 0$ as $t \to \infty$. Substitution of (2.16) into (2.15) determines the eigenvalues λ as the solutions of

$$\begin{aligned} |\,\gamma A - \lambda I\,| &= \begin{vmatrix} \gamma f_u - \lambda & \gamma f_v \\ \gamma g_u & \gamma g_v - \lambda \end{vmatrix} = 0 \\ \Rightarrow \quad \lambda^2 - \gamma(f_u + g_v)\lambda + \gamma^2(f_u g_v - f_v g_u) &= 0, \end{aligned} \tag{2.17}$$

so

$$\lambda_1, \lambda_2 = \frac{1}{2}\gamma\left[(f_u + g_v) \pm \left\{(f_u + g_v)^2 - 4(f_u g_v - f_v g_u)\right\}^{1/2}\right]. \tag{2.18}$$

Linear stability, that is, $\mathrm{Re}\,\lambda < 0$, is guaranteed if

$$\mathrm{tr}\,A = f_u + g_v < 0, \quad |\,A\,| = f_u g_v - f_v g_u > 0. \tag{2.19}$$

Since (u_0, v_0) are functions of the parameters of the kinetics, these inequalities thus impose certain constraints on the parameters. Note that for all cases in Figure 2.2 in the neighbourhood of the steady state, $f_u > 0$, $g_v < 0$, and for Figure 2.2(a) $f_v > 0$, $g_u < 0$ while for Figure 2.2(b) to (d) $f_v < 0$, $g_u > 0$. So tr A and $|\,A\,|$ could be positive or negative: here we are only concerned with the conditions and parameter ranges which satisfy (2.19).

Now consider the full reaction diffusion system (2.11) and again linearise about the steady state, which with (2.14) is $\mathbf{w} = 0$, to get

$$\mathbf{w}_t = \gamma A\mathbf{w} + D\nabla^2\mathbf{w}, \quad D = \begin{pmatrix} 1 & 0 \\ 0 & d \end{pmatrix}. \tag{2.20}$$

To solve this system of equations subject to the boundary conditions (2.11) we first define $\mathbf{W}(\mathbf{r})$ to be the time-independent solution of the spatial eigenvalue problem defined by

$$\nabla^2\mathbf{W} + k^2\mathbf{W} = 0, \quad (\mathbf{n}\cdot\nabla)\mathbf{W} = 0 \quad \text{for} \quad \mathbf{r} \text{ on } \partial B, \tag{2.21}$$

where k is the eigenvalue. For example, if the domain is one-dimensional, say, $0 \le x \le a$, $\mathbf{W} \propto \cos(n\pi x/a)$ where n is an integer; this satisfies zero flux conditions at $x = 0$ and $x = a$. The eigenvalue in this case is $k = n\pi/a$. So, $1/k = a/n\pi$ is a measure of the wavelike pattern: the eigenvalue k is called the *wavenumber* and $1/k$ is proportional to the wavelength ω; $\omega = 2\pi/k = 2a/n$ in this example. From now on we shall refer to k in this context as the wavenumber. With finite domains there is a discrete set of possible wavenumbers since n is an integer.

Let $\mathbf{W}_k(\mathbf{r})$ be the eigenfunction corresponding to the wavenumber k. Each eigenfunction $\mathbf{W}_k$ satisfies zero flux boundary conditions. Because the problem is linear we now look for solutions $\mathbf{w}(\mathbf{r}, t)$ of (2.20) in the form

$$\mathbf{w}(\mathbf{r}, t) = \sum_k c_k e^{\lambda t}\mathbf{W}_k(\mathbf{r}), \tag{2.22}$$

where the constants c_k are determined by a Fourier expansion of the initial conditions in terms of $\mathbf{W}_k(\mathbf{r})$. λ is the eigenvalue which determines temporal growth. Substituting this form into (2.20) with (2.21) and cancelling $e^{\lambda t}$, we get, for each k,

$$\begin{aligned}\lambda\mathbf{W}_k &= \gamma A\mathbf{W}_k + D\nabla^2\mathbf{W}_k \\ &= \gamma A\mathbf{W}_k - Dk^2\mathbf{W}_k.\end{aligned}$$

We require nontrivial solutions for $\mathbf{W}_k$ so the λ are determined by the roots of the characteristic polynomial

$$|\,\lambda I - \gamma A + Dk^2\,| = 0.$$

Evaluating the determinant with A and D from (2.15) and (2.20) we get the eigenvalues $\lambda(k)$ as functions of the wavenumber k as the roots of

$$\begin{aligned}&\lambda^2 + \lambda[k^2(1+d) - \gamma(f_u + g_v)] + h(k^2) = 0, \\ &h(k^2) = dk^4 - \gamma(df_u + g_v)k^2 + \gamma^2|\,A\,|.\end{aligned} \tag{2.23}$$

The steady state (u_0, v_0) is linearly stable if both solutions of (2.23) have $\mathrm{Re}\,\lambda < 0$. We have already imposed the constraints that the steady state is stable in the absence of any spatial effects; that is, $\mathrm{Re}\,\lambda(k^2 = 0) < 0$. The quadratic (2.23) in this case is (2.17) and the requirement that $\mathrm{Re}\,\lambda < 0$ gave conditions (2.19). For the steady state to be unstable to *spatial* disturbances we require $\mathrm{Re}\,\lambda(k) > 0$ for some $k \neq 0$. This can happen if either the coefficient of λ in (2.23) is negative, or if $h(k^2) < 0$ for some $k \neq 0$. Since $(f_u + g_v) < 0$ from conditions (2.19) and $k^2(1+d) > 0$ for all $k \neq 0$ the

coefficient of λ, namely,

$$[k^2(1+d) - \gamma(f_u + g_v)] > 0,$$

so the only way $\mathrm{Re}\,\lambda(k^2)$ can be positive is if $h(k^2) < 0$ for some k. This is immediately clear from the solutions of (2.23), namely,

$$2\lambda = -[k^2(1+d) - \gamma(f_u + g_v)] \pm \{[k^2(1+d) - \gamma(f_u + g_v)]^2 - 4h(k^2)\}^{1/2}.$$

Since we required the determinant $|A| > 0$ from (2.19) the only possibility for $h(k^2)$ in (2.23) to be negative is if $(df_u + g_v) > 0$. Since $(f_u + g_v) < 0$ from (2.19) this implies that $d \neq 1$ and f_u and g_v must have opposite signs. So, a further requirement to those in (2.19) is

$$df_u + g_v > 0 \quad \Rightarrow \quad d \neq 1. \tag{2.24}$$

With the reaction kinetics giving the null clines in Figure 2.2 we noted that $f_u > 0$ and $g_v < 0$, so the first condition in (2.19) and the last inequality (2.24) require that the diffusion coefficient ratio $d > 1$. For example, in terms of the activator–inhibitor mechanism (2.8) this means that the inhibitor must diffuse faster than the activator as we noted above.

The inequality (2.24) is necessary but not sufficient for $\mathrm{Re}\,\lambda > 0$. For $h(k^2)$ to be negative for some nonzero k, the minimum $h_{\min}$ must be negative. From (2.23), elementary differentiation with respect to k^2 shows that

$$h_{\min} = \gamma^2 \left[|A| - \frac{(df_u + g_v)^2}{4d} \right], \quad k^2 = k_m^2 = \gamma \frac{df_u + g_v}{2d}. \tag{2.25}$$

Thus the condition that $h(k^2) < 0$ for some $k^2 \neq 0$ is

$$\frac{(df_u + g_v)^2}{4d} > |A|. \tag{2.26}$$

At bifurcation, when $h_{\min} = 0$, we require $|A| = (df_u + g_v)^2/4d$ and so for fixed kinetics parameters this defines a critical diffusion coefficient ratio $d_c (> 1)$ as the appropriate root of

$$d_c^2 f_u^2 + 2(2f_v g_u - f_u g_v) d_c + g_v^2 = 0. \tag{2.27}$$

The critical wavenumber k_c is then given (using (2.26)) by

$$k_c^2 = \gamma \frac{d_c f_u + g_v}{2d_c} = \gamma \left[\frac{|A|}{d_c} \right]^{1/2} = \gamma \left[\frac{f_u g_v - f_v g_u}{d_c} \right]^{1/2}. \tag{2.28}$$

Figure 2.5(a) shows how $h(k^2)$ varies as a function of k^2 for various d.

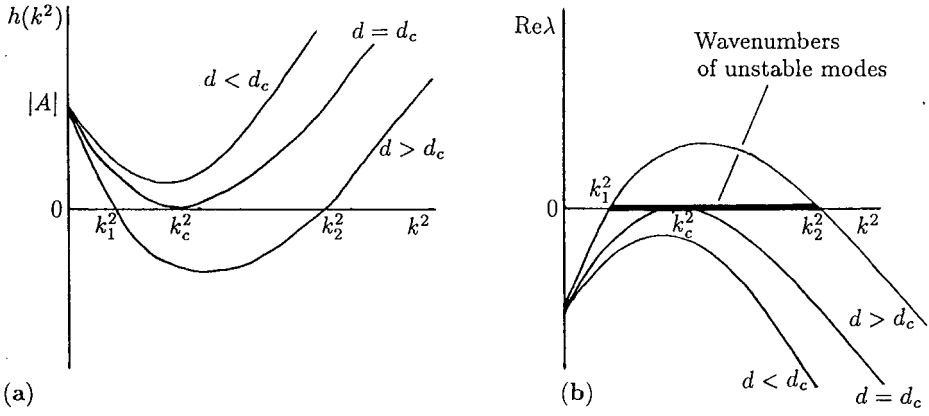

Figure 2.5. (**a**) Plot of $h(k^2)$ defined by (2.23) for typical kinetics illustrated in Figure 2.2. When the diffusion coefficient ratio d increases beyond the critical value d_c, $h(k^2)$ becomes negative for a finite range of $k^2 > 0$. (**b**) Plot of the largest of the eigenvalues $\lambda(k^2)$ from (2.23) as a function of k^2. When $d > d_c$ there is a range of wavenumbers $k_1^2 < k^2 < k_2^2$ which are linearly unstable.

Whenever $h(k^2) < 0$, (2.23) has a solution λ which is positive for the same range of wavenumbers that make $h < 0$. From (2.23) with $d > d_c$ the range of unstable wavenumbers $k_1^2 < k^2 < k_2^2$ is obtained from the zeros k_1^2 and k_2^2 of $h(k^2) = 0$ as

$$\begin{aligned} k_1^2 &= \frac{\gamma}{2d}\left[(df_u + g_v) - \{(df_u + g_v)^2 - 4d|\,A\,|\}^{1/2}\right] < k^2 \\ &< \frac{\gamma}{2d}\left[(df_u + g_v) + \{(df_u + g_v)^2 - 4d|\,A\,|\}^{1/2}\right] = k_2^2. \end{aligned} \tag{2.29}$$

Figure 2.5(b) plots a typical $\lambda(k^2)$ against k^2. The expression $\lambda = \lambda(k^2)$ is called a *dispersion relation*. We discuss the importance and use of dispersion relations in more detail in the next two sections. Note that, within the unstable range, $\mathrm{Re}\,\lambda(k^2) > 0$ has a maximum for the wavenumber k_m obtained from (2.25) with $d > d_c$. This implies that there is a fastest growing mode in the summation (2.22) for $\mathbf{w}$; this is an attribute we now exploit.

If we consider the solution $\mathbf{w}$ given by (2.22), the dominant contributions as t increases are those modes for which $\mathrm{Re}\,\lambda(k^2) > 0$ since all other modes tend to zero exponentially. From Figure 2.5, or analytically from (2.29), we determine the range, $k_1^2 < k^2 < k_2^2$, where $h(k^2) < 0$, and hence $\mathrm{Re}\,\lambda(k^2) > 0$, and so from (2.22)

$$\mathbf{w}(\mathbf{r}, t) \sim \sum_{k_1}^{k_2} c_k e^{\lambda(k^2)t} \mathbf{W}_k(\mathbf{r}) \quad \text{for large } t. \tag{2.30}$$

An analysis and graph of the dispersion relation are thus extremely informative in that they immediately say which eigenfunctions, that is, which spatial patterns, are linearly unstable and grow exponentially with time. We must keep in mind that, with finite domain eigenvalue problems, the wavenumbers are discrete and so only certain k in the range (2.29) are of relevance; we discuss the implications of this later.

The key assumption, and what in fact happens, is that these linearly unstable eigenfunctions in (2.30) which are growing exponentially with time will eventually be bounded by the nonlinear terms in the reaction diffusion equations and an ultimate steady state spatially inhomogeneous solution will emerge. A key element in this assumption is the existence of a confined set (or bounding domain) for the kinetics (see Chapter 3, Volume I). We would intuitively expect that if a confined set exists for the kinetics, the same set would also contain the solutions when diffusion is included. This is indeed the case and can be rigorously proved; see Smoller (1983). So, part of the analysis of a specific mechanism involves the demonstration of a confined set within the *positive* quadrant. A general nonlinear analysis for the evolution to the finite amplitude steady state spatial patterns is still lacking but singular perturbation analyses for d near the bifurcation value d_c have been carried out and a nonuniform spatially heterogeneous solution is indeed obtained (see, for example, Lara-Ochoa and Murray 1983, Zhu and Murray 1995). Singular perturbation analyses can be done near any of the critical parameters near bifurcation. There have now been many spatially inhomogeneous solutions evaluated numerically using a variety of specific reaction diffusion mechanisms; the numerical methods are now quite standard. The results presented in the next chapter illustrate some of the richness of pattern which can be generated.

To recap, we have now obtained conditions for the generation of spatial patterns by *two*-species reaction diffusion mechanisms of the form (2.11). For convenience we reproduce them here. Remembering that all derivatives are evaluated at the steady state (u_0, v_0), they are, from (2.19), (2.24) and (2.26),

$$\begin{aligned} &f_u + g_v < 0, \quad f_u g_v - f_v g_u > 0, \\ &df_u + g_v > 0, \quad (df_u + g_v)^2 - 4d(f_u g_v - f_v g_u) > 0. \end{aligned} \tag{2.31}$$

The derivatives f_u and g_v must be of opposite sign: with the reaction kinetics exhibited in Figure 2.2, $f_u > 0$, $g_v < 0$ so the first and third of (2.31) imply that the ratio of diffusion coefficients $d > 1$.

There are two possibilities for the cross-terms f_v and g_u since the only restriction is that $f_v g_u < 0$. So, we must have $f_v < 0$ and $g_u > 0$ or the other way round. These correspond to qualitatively different reactions. The two cases are illustrated schematically in Figure 2.6. Recall that the reactant which promotes growth in one is the activator and the other the inhibitor. In the case illustrated in Figure 2.6(a), u is the activator, which is also self-activating, while the inhibitor, v, inhibits not only u, but also itself. For pattern formation to take place the inhibitor must diffuse more quickly than the activator. In the case illustrated in Figure 2.6(b), v is the activator but is still self-inhibiting and diffuses more quickly. There is another difference between the two cases. The pattern grows along the unstable manifold associated with the positive eigenvalue. In Figure 2.6(a) this means that the two species are at high or low density in the same region as the pattern grows as in Figure 2.6(c); in case Figure 2.6(b) u is at a high density where v is low, and vice versa as in Figure 2.6(d). The qualitative features of the phase plane (just for the reaction terms) in the vicinity of the steady state are shown in Figure 2.6(e) and (f) for the two cases. The fact that the patterns are either in or out of phase has fundamental implications for biological applications.

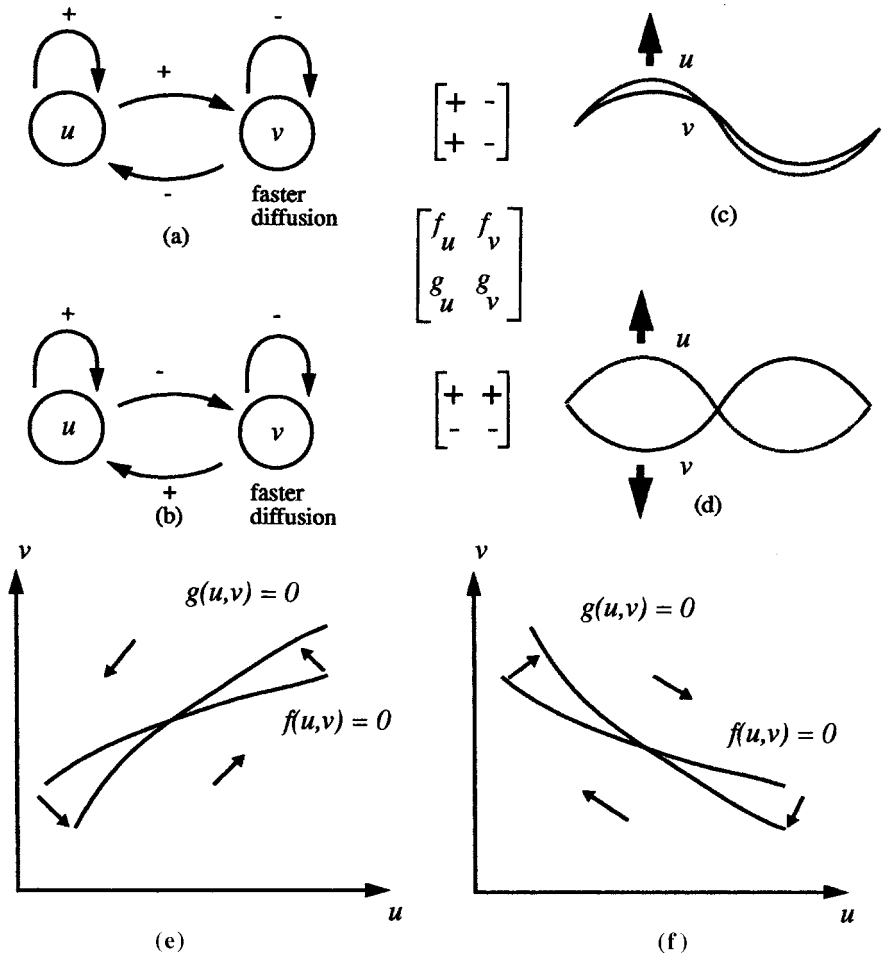

Figure 2.6. Schematic illustration of the two qualitatively different cases of diffusion driven instability. (**a**) self-activating u also activates v, which inhibits both reactants. The resulting initially growing pattern is shown in (**c**). (**b**) Here the self-activating u inhibits v but is itself activated by v with the resulting pattern illustrated in (**d**). The matrices give the signs of f_u, f_v, g_u, g_v evaluated at the steady state. (**e**) and (**f**) The reaction phase planes near the steady state. The arrows indicate the direction of change due to reaction (in the absence of diffusion). Case (**e**) corresponds to the interactions illustrated in (**a**) and (**c**) while that in (**f**) corresponds to the interactions illustrated in (**b**) and (**d**).

To get an intuitive feel for these two cases let us consider two different ecological predator–prey scenarios. In the first, that is, Figure 2.6(e), let u and v represent the prey and predator respectively. At high predator density prey numbers are reduced but at low densities their number is increased. Near the steady state the prey benefit from each other in that an increase in number is temporarily amplified. Predators decrease in numbers if the predator-to-prey ratio is high, but otherwise increase. Another example, from parasitology, is if v is a parasite dispersing via a motile host while u is a more sedentary host that is severely affected by the parasite. In these the interaction near the

steady state is as in Figure 2.6(a) with the local null clines and qualitative growth as in Figure 2.6(e).

A necessary condition for diffusion-driven instability in this predator–prey situation is that the predators disperse faster than the prey. In this case the patterns form as in Figure 2.6(c). Let us suppose there is a region of increased prey density. Without diffusion this would be damped out since the predators would temporarily increase and then drop back towards the steady state. However, with the predators diffusing it is possible that the local increase in predators (due to an increase in the prey) partially disperses and so is not strong enough to push the prey population back towards equilibrium. When predators disperse they lower the prey density in the neighbourhood. It is therefore possible to end up with clumps of high prey and predator populations interspersed with areas in which both densities are low. In the parasite analogy clumping of the sedentary prey (the host) coincides with areas of high parasite density. Hosts can also exist at high levels because the parasites continue to disperse into the nearby 'dead zone' in which there are few of this type of host. The scale on which patterning takes place depends on the ratio of the diffusion coefficients d.

Now consider the second type of interaction illustrated in Figures 2.6(b), (d) and (f). Again with a predator–prey situation let u now be the predator and v the prey. In this case the predators are 'autocatalytic' since when densities are close to the steady state, an increase in predator density is temporarily amplified, a not uncommon situation. For example, increased predator densities could improve hunting or reproductive efficiency. Another difference between this case and the first one is that it is now the prey that disperse at a faster rate.

Suppose again that there is a high prey density area. Without diffusion the predator numbers would increase and eventually make both populations return to the steady state. However, it could happen that the predators grow and reduce the prey population to a level below the steady state value (the temporary increase in prey is enough to prompt the autocatalytic growth of predators to kick in). This would result in a net flux of prey from neighbouring regions which in turn would cause the predator density to drop in those regions (as autocatalysis works in the other direction) thereby letting the prey populations grow above their steady state value. A pattern could become established in which areas of low predator/high prey supply with extra prey in those areas in which there are few prey and large numbers of predators. In effect, autocatalytic predators benefit both from being at a high density locally and also because nearby there are regions containing few predators which thus supply them with a constant extra flux of prey. Prey continue to flow towards regions of high predation because of the random nature of diffusion.

If the conditions (2.31) are satisfied there is a scale (γ)-dependent range of patterns, with wavenumbers defined by (2.29), which are linearly unstable. The spatial patterns which initially grow (exponentially) are those eigenfunctions $\mathbf{W}_k(\mathbf{r})$ with wavenumbers between k_1 and k_2 determined by (2.29), namely, those in (2.30). Note that the scale parameter γ plays a crucial role in these expressions, a point we consider further in the next section. Generally we would expect the kinetics and diffusion coefficients to be fixed. In the case of embryogenesis the natural variable parameter is then γ which reflects the size of the embryo or rather the embryonic domain (such as a developing limb bud) we are considering.

Diffusion-Driven Instability in Infinite Domains: Continuous Spectrum of Eigenvalues

In a finite domain the possible wavenumbers k and corresponding spatial wavelengths of allowable patterns are discrete and depend in part on the boundary conditions. In developmental biology the size of the embryo during the period of spatial patterning is often sufficiently large, relative to the pattern to be formed, that the 'boundaries' cannot play a major role in isolating specific wavelengths, as, for example, in the generation of patterns of hair, scale and feather primordia discussed in later chapters. Thus, for practical purposes the pattern formation domain is effectively infinite. Here we describe how to determine the spectrum of unstable eigenvalues for an infinite domain—it is easier than for a finite domain.

We start with the linearised system (2.20) and look for solutions in the form

$$\mathbf{w}(\mathbf{r}, t) \propto \exp[\lambda t + i\mathbf{k} \cdot \mathbf{r}],$$

where $\mathbf{k}$ is the wave vector with magnitude $k = |\,\mathbf{k}\,|$. Substitution into (2.20) again gives

$$|\,\lambda I - \gamma A + Dk^2\,| = 0$$

and so the dispersion relation giving λ in terms of the wavenumbers k is again given by (2.23). The range of eigenvalues for which $\mathrm{Re}\,\lambda(k^2) > 0$ is again given by (2.29). The crucial difference between the situation here and that for a finite domain is that there is always a spatial pattern if, in (2.29), $0 < k_1^2 < k_2^2$ since we are not restricted to a discrete class of k^2 defined by the eigenvalue problem (2.21). So, at bifurcation when k_c^2, given by (2.28), is linearly unstable the mechanism will evolve to a spatial pattern with the critical wavelength $\omega_c = 2\pi/k_c$. Thus the wavelength with the maximum exponential growth in Figure 2.5(b) will be the pattern which generally emerges at least in one dimension: it is not always the case and depends on the number of unstable modes and initial conditions. In the next chapter on biological applications we shall see that the difference between a finite domain and an effectively infinite one has important biological implications: finite domains put considerable restrictions on the allowable patterns.

2.4 Detailed Analysis of Pattern Initiation in a Reaction Diffusion Mechanism

Here we consider, by way of example, a specific two-species reaction diffusion system and carry out the detailed analysis. We lay the groundwork in this section for the subsequent applications to real biological pattern formation problems. We calculate the eigenfunctions, obtain the specific conditions on the parameters necessary to initiate spatial patterns and determine the wavenumbers and wavelengths of the spatial disturbances which initially grow exponentially.

We study the simplest reaction diffusion mechanism (2.7), first in one space dimension; namely,

$$u_t = \gamma f(u, v) + u_{xx} = \gamma(a - u + u^2 v) + u_{xx},$$
$$v_t = \gamma g(u, v) + d v_{xx} = \gamma(b - u^2 v) + d v_{xx}. \tag{2.32}$$

The kinetics null clines $f = 0$ and $g = 0$ are illustrated in Figure 2.2(a). The uniform positive steady state (u_0, v_0) is

$$u_0 = a + b, \quad v_0 = \frac{b}{(a+b)^2}, \quad b > 0, \quad a + b > 0 \tag{2.33}$$

and, at the steady state,

$$f_u = \frac{b-a}{a+b}, \quad f_v = (a+b)^2 > 0, \quad g_u = \frac{-2b}{a+b} < 0,$$
$$g_v = -(a+b)^2 < 0, \quad f_u g_v - f_v g_u = (a+b)^2 > 0. \tag{2.34}$$

Since f_u and g_v must have opposite signs we must have $b > a$. With these expressions, conditions (2.31) require

$$\begin{aligned} &f_u + g_v < 0 \quad \Rightarrow \quad 0 < b - a < (a+b)^3, \\ &f_u g_v - f_v g_u > 0 \quad \Rightarrow \quad (a+b)^2 > 0, \\ &d f_u + g_v > 0 \quad \Rightarrow \quad d(b-a) > (a+b)^3, \\ &(d f_u + g_v)^2 - 4d(f_u g_v - f_v g_u) > 0 \\ &\Rightarrow \quad [d(b-a) - (a+b)^3]^2 > 4d(a+b)^4. \end{aligned} \tag{2.35}$$

These inequalities define a domain in (a, b, d) parameter space, called the pattern formation space (or Turing space), within which the mechanism is unstable to certain spatial disturbances of given wavenumbers k, which we now determine.

Consider the related eigenvalue problem (2.21) and let us choose the domain to be $x \in (0, p)$ with $p > 0$. We then have

$$\mathbf{W}_{xx} + k^2 \mathbf{W} = 0, \quad \mathbf{W}_x = 0 \text{ for } x = 0, p \tag{2.36}$$

the solutions of which are

$$\mathbf{W}_n(x) = \mathbf{A}_n \cos(n\pi x/p), \quad n = \pm 1, \pm 2, \ldots, \tag{2.37}$$

where the $\mathbf{A}_n$ are arbitrary constants. The eigenvalues are the *discrete* wavenumbers $k = n\pi/p$. Whenever (2.34) are satisfied and there is a range of wavenumbers $k = n\pi/p$ lying within the bounds defined by (2.29), then the corresponding eigenfunctions $\mathbf{W}_n$ are linearly unstable. Thus the eigenfunctions (2.37) with wavelengths $\omega = 2\pi/k = 2p/n$ are the ones which initially grow with time like $\exp\{\lambda([n\pi/p]^2)t\}$. The band of wavenumbers from (2.29), with (2.34), is given by

$$\gamma L(a,b,d) = k_1^2 < k^2 = \left(\frac{n\pi}{p}\right)^2 < k_2^2 = \gamma M(a,b,d)$$

$$L = \frac{[d(b-a)-(a+b)^3] - \{[d(b-a)-(a+b)^3]^2 - 4d(a+b)^4\}^{1/2}}{2d(a+b)}, \tag{2.38}$$

$$M = \frac{[d(b-a)-(a+b)^3] + \{[d(b-a)-(a+b)^3]^2 - 4d(a+b)^4\}^{1/2}}{2d(a+b)}.$$

In terms of the wavelength $\omega = 2\pi/k$, the range of unstable modes $\mathbf{W}_n$ have wavelengths bounded by ω_1 and ω_2, where

$$\frac{4\pi^2}{\gamma L(a,b,d)} = \omega_1^2 > \omega^2 = \left(\frac{2p}{n}\right)^2 > \omega_2^2 = \frac{4\pi^2}{\gamma M(a,b,d)}. \tag{2.39}$$

Note in (2.38) the importance of scale, quantified by γ. The smallest wavenumber is π/p; that is, $n = 1$. For fixed parameters a, b and d, if γ is sufficiently small (2.38) says that there is *no allowable* k in the range, and hence no mode $\mathbf{W}_n$ in (2.37), which can be driven unstable. This means that all modes in the solution $\mathbf{w}$ in (2.30) tend to zero exponentially and the steady state is stable. We discuss this important role of scale in more detail below.

From (2.30) the spatially heterogeneous solution which emerges is the sum of the unstable modes, namely,

$$\mathbf{w}(x,t) \sim \sum_{n_1}^{n_2} \mathbf{C}_n \exp\left[\lambda\left(\frac{n^2\pi^2}{p^2}\right)t\right] \cos\frac{n\pi x}{p}, \tag{2.40}$$

where λ is given by the positive solution of the quadratic (2.23) with the derivatives from (2.34), n_1 is the smallest integer greater than or equal to pk_1/π, n_2 the largest integer less than or equal to pk_2/π and $\mathbf{C}_n$ are constants which are determined by a Fourier series analysis of the initial conditions for $\mathbf{w}$. Initial conditions in any biological context involve a certain stochasticity and so it is inevitable that the Fourier spectrum will contain the whole range of Fourier modes; that is, the $\mathbf{C}_n$ are nonzero. We can therefore assume at this stage that γ is sufficiently large to ensure that allowable wavenumbers exist in the unstable range of k. Before discussing the possible patterns which emerge let us first obtain the corresponding two-dimensional result.

Consider the two-dimensional domain defined by $0 < x < p$, $0 < y < q$ whose rectangular boundary we denote by ∂B. The spatial eigenvalue problem in place of that in (2.36) is now

$$\nabla^2\mathbf{W} + k^2\mathbf{W} = 0, \quad (\mathbf{n}\cdot\nabla)\mathbf{W} = 0 \quad \text{for} \quad (x,y) \text{ on } \partial B \tag{2.41}$$

the eigenfunctions of which are

$$\mathbf{W}_{p,q}(x,y) = \mathbf{C}_{n,m} \cos\frac{n\pi x}{p} \cos\frac{m\pi y}{q}, \quad k^2 = \pi^2\left(\frac{n^2}{p^2} + \frac{m^2}{q^2}\right), \tag{2.42}$$

where n and m are integers. The two-dimensional modes $\mathbf{W}_k(x, y)$ which are linearly unstable are those with wavenumbers k, defined by the last equation, lying within the unstable band of wavenumbers defined in terms of a, b and d by (2.38). We again assume that γ is sufficiently large so that the range of unstable wavenumbers contains at least one possible mode. Now the unstable spatially patterned solution is given by (2.30) with (2.42) as

$$\begin{aligned} \mathbf{w}(x, y, t) &\sim \sum_{n,m} \mathbf{C}_{n,m} e^{\lambda(k^2)t} \cos\frac{n\pi x}{p} \cos\frac{m\pi y}{q}, \\ \gamma L(a, b, d) = k_1^2 < k^2 &= \pi^2 \left(\frac{n^2}{p^2} + \frac{m^2}{q^2}\right) < k_2^2 = \gamma M(a, b, d), \end{aligned} \tag{2.43}$$

where the summation is over all pairs (n, m) which satisfy the inequality, L and M are defined by (2.38) as before and $\lambda(k^2)$ is again the positive solution of (2.23) with the expressions for the derivatives of f and g given by (2.34). As t increases a spatial pattern evolves which is initially made up of the modes in (2.43).

Now consider the type of spatial patterns we might expect from the unstable solutions in (2.40) and (2.43). Suppose first that the domain size, as measured by γ, is such that the range of unstable wavenumbers in (2.38) admits only the wavenumber $n = 1$: the corresponding dispersion relation for λ in terms of the wavelengths $\omega = 2p/n$ is illustrated in Figure 2.7(a). The only unstable mode, from (2.37) is then $\cos(\pi x/p)$ and the growing instability is given by (2.40) as

$$\mathbf{w}(x, t) \sim \mathbf{C}_1 \exp\left[\lambda\left(\frac{\pi^2}{p^2}\right)t\right] \cos\frac{\pi x}{p},$$

where λ is the positive root of the quadratic (2.23) with f_u, f_v, g_u and g_v from (2.34) and with $k^2 = (\pi/p)^2$. Here all other modes decay exponentially with time. We can only determine the $\mathbf{C}_1$ from initial conditions. To get an intuitive understanding for what is going on, let us simply take $\mathbf{C}_1$ as $(\varepsilon, \varepsilon)$ for some small positive ε and consider the morphogen u; that is, from the last equation and the definition of $\mathbf{w}$ from (2.14),

$$u(x, t) \sim u_0 + \varepsilon \exp\left[\lambda\left(\frac{\pi^2}{p^2}\right)t\right] \cos\frac{\pi x}{p}. \tag{2.44}$$

This unstable mode, which is the dominant solution which emerges as t increases, is illustrated in Figure 2.7(b). In other words, this is the pattern predicted by the dispersion relation in Figure 2.7(a).

Clearly if the exponentially growing solution were valid for all time it would imply $u \to \infty$ as $t \to \infty$. For the mechanism (2.32), the kinetics has a confined set, within the positive quadrant, which bounds the solution. So the solution in the last equation must be bounded and lie in the positive quadrant. We hypothesise that this growing solution eventually settles down to a spatial pattern which is similar to the single cosine mode shown in Figure 2.7(b). As mentioned before, singular perturbation analyses in the

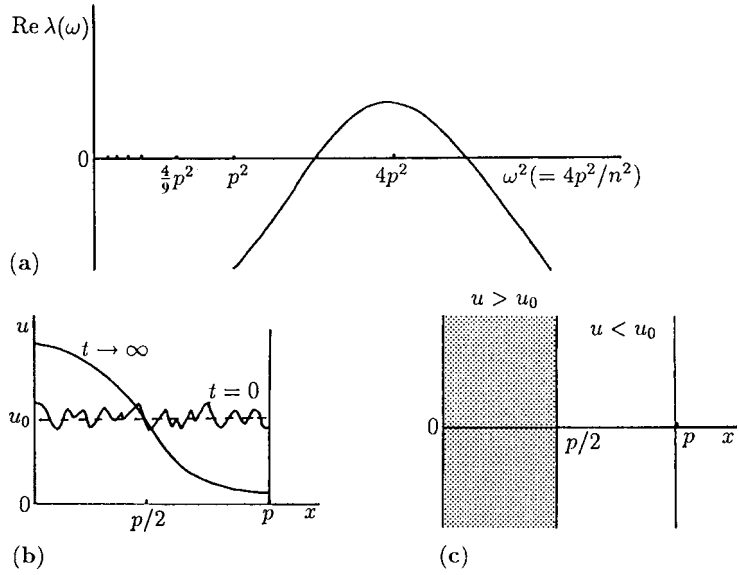

Figure 2.7. (**a**) Typical dispersion relation for the growth factor $\mathrm{Re}\,\lambda$ as a function of the wavelength ω obtained from a linearization about the steady state. The only mode which is linearly unstable has $n = 1$; all other modes have $\mathrm{Re}\,\lambda < 0$. (**b**) The temporally growing linear mode which eventually evolves from random initial conditions into a finite amplitude spatial pattern such as shown in (**c**), where the shaded area corresponds to a concentration higher than the steady state u_0 and the unshaded area to a concentration lower than the steady state value.

vicinity of the bifurcation in one of the parameters, for example, near the critical domain size for γ, such that a single wavenumber is just unstable, or when the critical diffusion coefficient ratio is near d_c, bear this out as do the many numerical simulations of the full nonlinear equations. Figure 2.7(c) is a useful way of presenting spatial patterned results for reaction diffusion mechanisms—the shaded region represents a concentration above the steady state value while the unshaded region represents concentrations below the steady state value. As we shall see, this simple way of presenting the results is very useful in the application of chemical prepattern theory to patterning problems in developmental biology, where it is postulated that cells differentiate when one of the morphogen concentrations is above (or below) some threshold level.

Let us now suppose that the domain size is doubled, say. With the definition of γ chosen to represent scale this is equivalent to multiplying the original γ by 4 since in the one-dimensional situation $\sqrt{\gamma}$ is proportional to size, that is, the length here, of the domain. This means that the dispersion relation and the unstable range are simply moved along the k^2-axis or along the ω^2-axis. Suppose the original $\gamma = \gamma_1$. The inequalities (2.38) determine the unstable modes as those with wavelengths $\omega(= 2\pi/k)$ determined by (2.39); namely,

$$\frac{4\pi^2}{\gamma_1 L(a,b,d)} > \omega^2 > \frac{4\pi^2}{\gamma_1 M(a,b,d)}. \tag{2.45}$$

Let this be the case illustrated in Figure 2.7(a) and which gives rise to the pattern in Figure 2.7(c). Now let the domain double in size. We consider exactly the same domain as in Figure 2.7 but with an increased γ to $4\gamma_1$. This is equivalent to having the same γ_1 but with a domain 4 times that in Figure 2.7. We choose the former means of representing a change in scale. The equivalent dispersion relation is now illustrated in Figure 2.8(a)—it is just the original one of Figure 2.7(a) moved along so that the wavelength of the excited or unstable mode now has $\omega = p$; that is, $n = 2$. The equivalent spatial pattern is then as in Figure 2.8(b). As we shall see in the applications chapters which follow, it is a

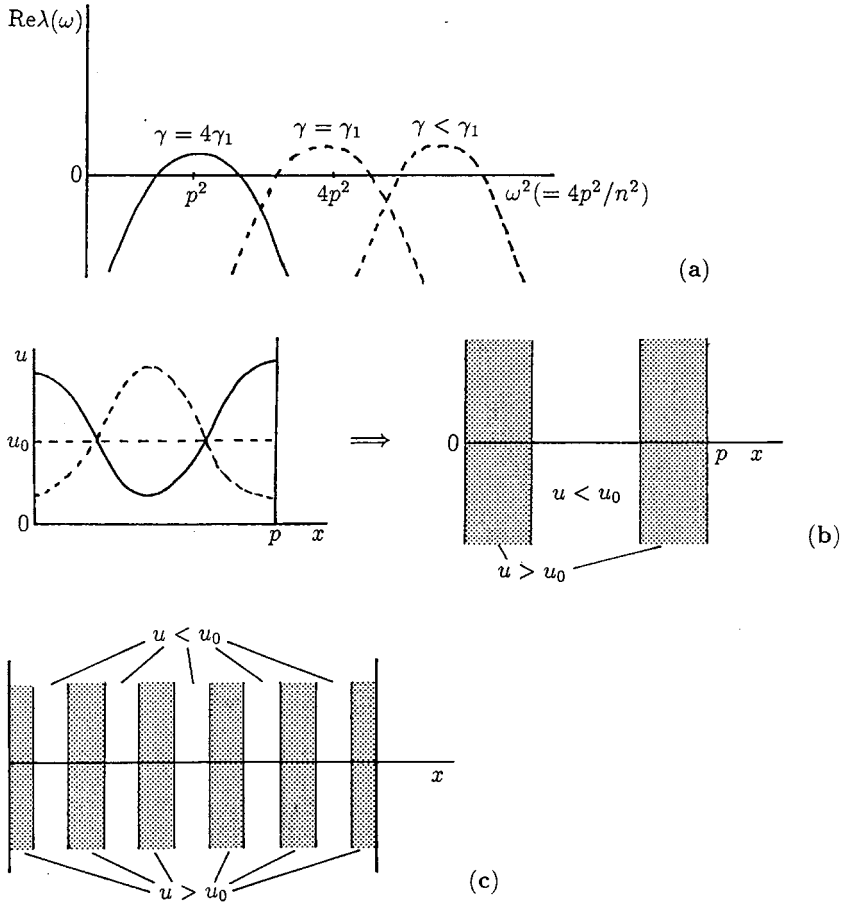

Figure 2.8. (**a**) Dispersion relation Re λ as a function of the wavelength ω when the single mode with $n = 2$ is unstable for a domain size $4\gamma_1$; the dashed curves are those with $\gamma = \gamma_1$ and $\gamma < \gamma_c < \gamma_1$, where γ_c is the critical bifurcation scale value of the domain that will not admit any heterogeneous pattern. (**b**) The spatial pattern in the morphogen u predicted by the dispersion relation in (**a**). The dashed line, the mirror image about $u = u_0$, is also an allowable form of this solution. The initial conditions determine which pattern is obtained. (**c**) The spatial pattern obtained when the domain is sufficiently large to fit in the number of unstable modes equivalent to $n = 10$: the shaded regions represent morphogen levels $u > u_0$, the uniform steady state.

particularly convenient way, when presenting spatial patterned solutions, to incorporate scale solely via a change in γ.

We can thus see with this example how the patterning process works as regards domain size. There is a basic wavelength picked out by the analysis for a given $\gamma = \gamma_1$, in this example that with $n = 1$. As the domain grows it eventually can incorporate the pattern with $n = 2$ and progressively higher modes the larger the domain, as shown in Figure 2.8(c). In the same way if the domain is sufficiently small there is clearly a $\gamma = \gamma_c$ such that the dispersion relation, now moved to the right in Figure 2.8(a), will not even admit the wavelength with $n = 1$. In this case no mode is unstable and so no spatial pattern can be generated. The concept of a critical domain size for the existence of spatial pattern is an important one both in developmental biology, and in spatially dependent ecological models as we show later.

Note in Figure 2.8(b) the two possible solutions for the same parameters and zero flux boundary conditions. Which of these is obtained depends on the bias in the initial conditions. Their existence poses certain conceptual difficulties from a developmental biology point of view within the context of positional information. If cells differentiate when the morphogen concentration is larger than some threshold then the differentiated cell pattern is obviously different for each of the two possible solutions. Development, however, is a sequential process and carries with it its own history so, a previous stage generally cues the next. In the context of reaction diffusion models this implies a bias in the initial conditions towards one of the patterns.

Now consider the two-dimensional problem with a dispersion relation such that the unstable modes are given by (2.43). Here the situation is not so straightforward since for a given γ, representing the *scale*, the actual modes which are unstable now depend on the domain *geometry* as measured by the length p and the width q. Referring to (2.43), first note that if the width is sufficiently small, that is, q is small enough, even the first mode with $m = 1$ lies outside the unstable range. The problem is then equivalent to the above one-dimensional situation. As the width increases, that is, q increases, genuine two-dimensional modes with $n \neq 0$ and $m \neq 0$ become unstable since

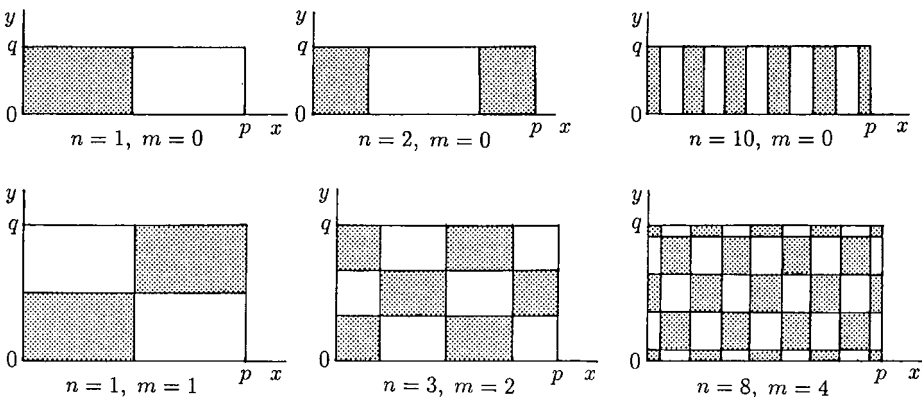

Figure 2.9. Typical two-dimensional spatial patterns indicated by the linearly unstable solution (2.43) when various wavenumbers are in the unstable range. The shaded regions are where $u > u_0$, the uniform steady state.

$\pi^2(n^2/p^2 + m^2/q^2)$ lies in the range of unstable wavenumbers. Figure 2.9 illustrates typical temporally growing spatial patterns indicated by (2.43) with various nonzero n and m.

Regular Planar Tesselation Patterns

The linear patterns illustrated in the last figure arise from the simplest two-dimensional eigenfunctions of (2.41). Less simple domains require the solutions of

$$\nabla^2\psi + k^2\psi = 0, \quad (\mathbf{n}\cdot\nabla)\psi = 0 \quad \text{for} \quad \mathbf{r} \text{ on } \partial B. \tag{2.46}$$

Except for simple geometries the analysis quickly becomes quite complicated. Even for circular domains the eigenvalues have to be determined numerically. There are, however, some elementary solutions for symmetric domains which tesselate the plane, namely, squares, hexagons, rhombi and, by subdivision, triangles; these were found by Christopherson (1940). In other words we can cover the complete plane with, for example, regular hexagonal tiles. (The basic symmetry group of regular polygons are hexagons, squares and rhombi, with, of course, triangles, which are subunits of these.) Hexagonal patterns, as we shall see, are common in many real developmental situations—feather distribution on the skin of birds is just one example (just look at the skin of a plucked chicken). Refer also to Figure 2.11 below where a variety of experimentally obtained patterns is shown. Thus we want solutions ψ where the unit cell, with zero flux conditions on its boundary, is one of the regular tesselations which can cover the plane. That is, we want solutions which are *cell* periodic; here the word 'cell' is, of course, meant as the unit of tesselation.

The solution of (2.46) for a hexagon is

$$\begin{aligned}\psi(x, y) &= \frac{\cos k\left(\frac{\sqrt{3}y}{2} + \frac{x}{2}\right) + \cos k\left(\frac{\sqrt{3}y}{2} - \frac{x}{2}\right) + \cos kx}{3} \\ &= \frac{\cos\left\{kr\sin\left(\theta + \frac{\pi}{6}\right)\right\} + \cos\left\{kr\sin\left(\theta - \frac{\pi}{6}\right)\right\} + \cos\left\{kr\sin\left(\theta - \frac{\pi}{2}\right)\right\}}{3}.\end{aligned} \tag{2.47}$$

From (2.46), a linear equation, ψ is independent to the extent of multiplication by an arbitrary constant: the form chosen here makes $\psi = 1$ at the origin. This solution satisfies zero flux boundary conditions on the hexagonal symmetry boundaries if $k = n\pi, n = \pm1, \pm2, \ldots$. Figure 2.10(a) shows the type of pattern the solution can generate.

The polar coordinate form shows the invariance to hexagonal rotation, that is, invariance to rotation by $\pi/3$, as it must. That is,

$$\psi(r, \theta) = \psi\left(r, \theta + \frac{\pi}{3}\right) = H\psi(r, \theta) = \psi(r, \theta),$$

where H is the hexagonal rotation operator.

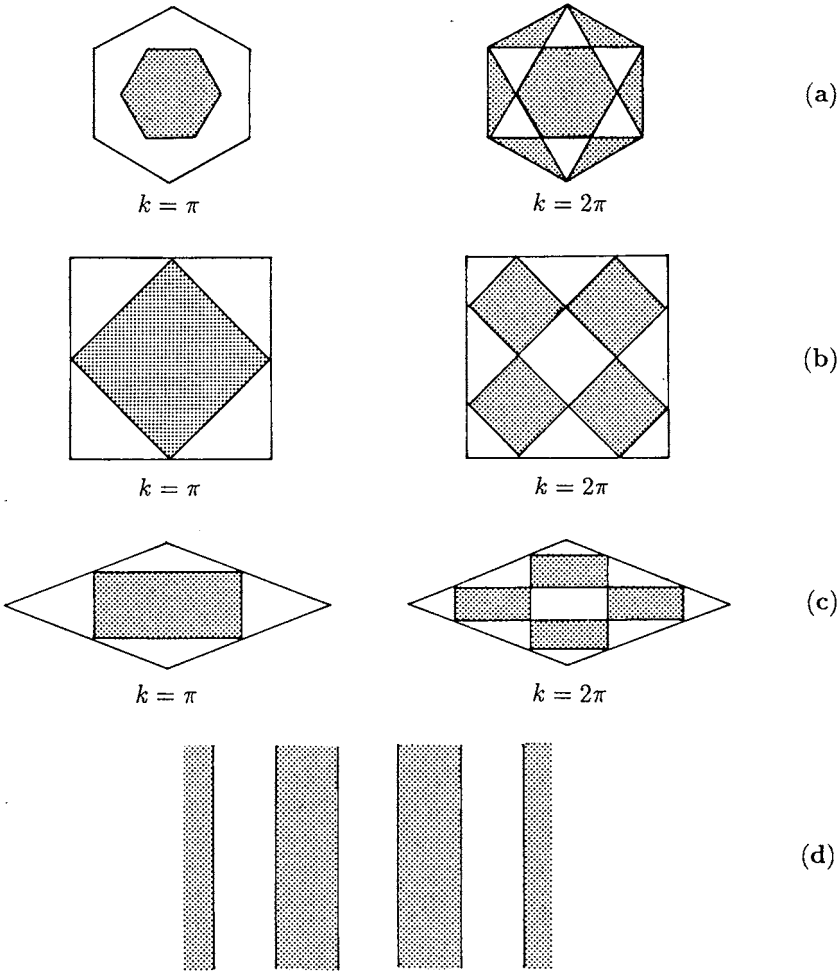

Figure 2.10. (**a**) Patterns which are obtained with the solution (2.47) with $k = \pi$ and $k = 2\pi$. The shaded region is where $\psi > 0$ and the unshaded region where $\psi < 0$. (**b**) Patterns generated by the solution (2.48) for a square tesselation with $k = \pi$ and $k = 2\pi$. (**c**) Rhombic patterns from (2.49) with $k = \pi$ and $k = 2\pi$. (**d**) One-dimensional roll patterns from (2.50).

The solution for the square is

$$\begin{aligned}\psi(x, y) &= \frac{\cos kx + \cos ky}{2} \\ &= \frac{\cos(kr\cos\theta) + \cos(kr\sin\theta)}{2},\end{aligned} \tag{2.48}$$

where $k = \pm 1, \pm 2 \ldots$ and $\psi(0, 0) = 1$. This solution is square rotationally invariant since

$$\psi(r,\theta) = \psi\left(r,\theta+\frac{\pi}{2}\right) = S\psi(r,\theta) = \psi(r,\theta),$$

where S is the square rotational operator. Typical patterns are illustrated in Figure 2.10(b).

The solution for the rhombus is

$$\begin{aligned}\psi(x,y) &= \frac{\cos kx + \cos\{k(x\cos\phi + y\sin\phi)\}}{2} \\ &= \frac{\cos\{kr\cos\theta\} + \cos\{kr\cos(\theta-\phi)\}}{2},\end{aligned} \tag{2.49}$$

where ϕ is the rhombus angle and again $k = \pm1, \pm2, \ldots$. This solution is invariant under a rhombic rotation; that is,

$$\psi(r,\theta;\phi) = \psi(r,\theta+\pi;\phi) = R\psi(r,\theta;\phi),$$

where R is the rhombic rotation operator. Illustrative patterns are shown in Figure 2.10(c).

A further cell periodic solution is the one-dimensional version of the square; that is, there is only variation in x. The solutions here are of the form

$$\psi(x,y) = \cos kx, \quad k = n\pi, \quad n = \pm1, \pm2, \ldots \tag{2.50}$$

and represent rolls with patterns as in Figure 2.10(d). These, of course, are simply the one-dimensional solutions (2.37).

When the full nonlinear equations are solved numerically with initial conditions taken to be small random perturbations about the steady state, linear theory turns out to be a good predictor of the ultimate steady state in the one-dimensional situation, particularly if the unstable modes have large wavelengths, that is, small wavenumbers. With larger wavenumbers the predictions are less reliable—and even more so with two-dimensional structures. Since the equations we have studied are linear and invariant when multiplied by a constant, we can have equivalent solutions which are simply mirror images in the line $u = u_0$; refer to Figure 2.8(b). Thus the pattern that evolves depends on the initial conditions and the final pattern tends to be the one closest to the initial conditions. There is, in a sense, a basin of attraction for the spatial patterns as regards the initial conditions. Once again near bifurcation situations singular perturbation analysis indicates nonlinear patterns closely related to the linear predictions. In general, however, away from the bifurcation boundaries linear predictions are much less reliable; see the computed patterns exhibited in the next chapter. Except for the simplest patterns, we should really use linear theory for two and three dimensions only as a guide to the wealth of patterns which can be generated by pattern formation mechanisms. Linear theory does, however, determine parameter ranges for pattern generation.

Figure 2.10 shows a selection of regular patterns that can be formed by reaction diffusion equations based on linear theory. Mathematically (and experimentally of course) a key question is which of these will be formed from given initial conditions. If one pattern is formed, variation of which parameters will effect changing to another? To de-

termine which of the various possible patterns—hexagons, rhombi, squares or rolls—will be stable we have to go beyond linear theory and carry out a weakly nonlinear analysis; that is, the parameters are such that they are close to the bifurcation boundary from homogeneity to heterogeneity. When we do such a nonlinear analysis we can determine the conditions on the parameters for stability of these steady state spatially heterogeneous solutions. This has been done for reaction diffusion equations by Ermentrout (1991) and Nagorcka and Mooney (1992) using a multi-scale singular perturbation analysis. Other pattern formation mechanisms, namely, cell-chemotaxis and mechanical mechanisms for pattern formation were studied by Zhu and Murray (1995). The latter compare chemotaxis systems and their patterning potential with reaction diffusion systems. Zhu and Murray (1995) were particularly interested in determining the parameter spaces which give rise to stable stripes, spots, squares and hexagons and their spatial characteristics such as wavelength and so on.

In the case of spots they could also determine which of the tessalation spot arrangement patterns would be stable. They compared the robustness and sensitivity of different models and confirmed the results with extensive numerical simulations of the equations. The analytical technique is well established but the details are fairly complex. Zhu and Murray (1995) show from their numerical study of the equations how the transition takes place from stripes to spots and then to hexagonal patterns and the converse pathway how hexagons become unstable and eventually end up in stripes. The hexagons in effect become elongated and rhombic in character with the spots lining up in lines and eventually fusing; it makes intuitive sense. The analytical procedure near bifurcation is referred to as weakly nonlinear stability analysis, an extensive review of which is given by Wollkind et al. (1994). Generally the form of the interaction kinetics plays a major role in what patterns are obtained. Cubic interactions tend to favour stripes while quadratic interactions tend to produce spots. When different boundary conditions (other than zero flux ones) are used the patterns obtained can be very different and less predictable. Barrio et al. (1999) investigated the effect of these and the role of the nonlinearities in the patterns obtained. From extensive numerical simulations they sugggest that such reaction diffusion mechanisms could play a role in some of the complex patterns observed on fish.

The patterns we have discussed up to now have mainly been regular in the sense that they are stripes, spots, hexagonal patterns and so on. Reaction diffusion systems can generate an enormous range of irregular patterns as we shall see in the following chapter where we discuss a few practical examples. The recent article by Meinhardt (2000: see also other references there) discusses complex patterns and in particular the application of reaction diffusion mechanisms to patterns of gene activation, a subject not treated in this book. He also reviews other important applications not treated here such as branching structures in plant morphology.

In the analyses of the pattern formation potential of reaction diffusion systems here the reactants, or morphogens, must have different diffusion coefficients. In many developmental situations there are often preferred directions in which the diffusion of the same morphogen may have different values in different directions; that is, the diffusion is anisotropic. Although we do not discuss it here, this can have, as we would expect, a marked affect on the patterns formed in a Turing instability of the uniform state (see Exercise 10).

It has been known for a long time, from the 1970's in fact, from many numerical studies that reaction diffusion systems can produce steady state finite amplitude spatial patterns. It is only in the last 10 years, however, that such steady state patterns, sometimes called Turing structures or Turing patterns, have been found experimentally. The experimental breakthrough started in 1989; see Ouyang et al. (1990, 1993), Castets et al. (1990), Ouyang and Swinney (1991), Gunaratne et al. (1994), De Kepper et al. (1994) and other references in these articles. The last two are good reviews to get an overall picture of some of these developments. The latter also describe the complex structures which are obtained when the Turing structures interact with travelling waves; they can be highly complex with such phenomena as spatiotemporal intermittency and spot splitting to form more complex patterns and so on. Ouyang and Swinney (1991) experimentally demonstrate the transition from a uniform state to hexagonal and eventually striped patterns; the transition is similar to that found by Zhu and Murray (1995) for both reaction diffusion and cell-chemotaxis pattern formation mechanisms. Since these early experimental studies, Turing patterns have been found with several quite different reaction systems; the details of the chemistry and experimental arrangements are given in detail in the papers. Figure 2.11 shows chemical Turing patterns obtained experimentally with a chlorite-iodide-malonic acid reaction diffusion system from Gunaratne et al. (1994). Note the small size of the domain and the accurately defined wavelength of the patterns which vary from 0.11 mm to 0.18 mm; these are certainly in the range we would expect of many morphogenetic situations and clearly demonstrate the potential for fine-scale delineation of pattern with reaction diffusion mechanisms and, from the theoretical studies of Zhu and Murray (1994) with other pattern generators. That they are of morphogenetic scale, in the case of the developing chick limb, at the time of the patterning associated with cartilage formation the width of the limb bud is of the order of 2 mm (see the discussion on a limb bud patterning scenario in Chapter 6). Wollkind and Stephenson (2000a,b) give a thorough and comprehensive discussion of the various transitions between patterns, including the black eye pattern shown in Figure 2.11. They specifically study the chlorite-iodide-malonic acid reaction system which was used in the experiments and importantly compare their results with experiment. They also relate these transitions between symmetry breaking structures in the chemical system to similar ones in quite different scientific contexts.

The application of reaction diffusion pattern generation to specific developmental biology problems is often within the context of a prepattern theory whereby cells differentiate according to the level of the morphogen concentration in which they find themselves. If the spatial patterns is quite distinct, as described above or with relatively large gradients, less sensitive tuning is required of the cells in order to carry out their assigned roles than if the pattern variation or the concentration gradients are small. It is perhaps useful therefore to try to get a quantitative measure of spatial heterogeneity, which is meaningful biologically, so as to compare different mechanisms. Another biologically relevant method will be discussed in the next section.

Berding (1987) introduced a 'heterogeneity' function for the spatial patterns generated by reaction diffusion systems with zero flux boundary conditions. Suppose the general mechanism (2.10), in one space variable, is diffusionally unstable and the solutions evolve to spatially inhomogeneous steady state solutions $U(x)$ and $V(x)$ as $t \to \infty$. With the definition of γ in (2.6) proportional to the square of the domain length we can

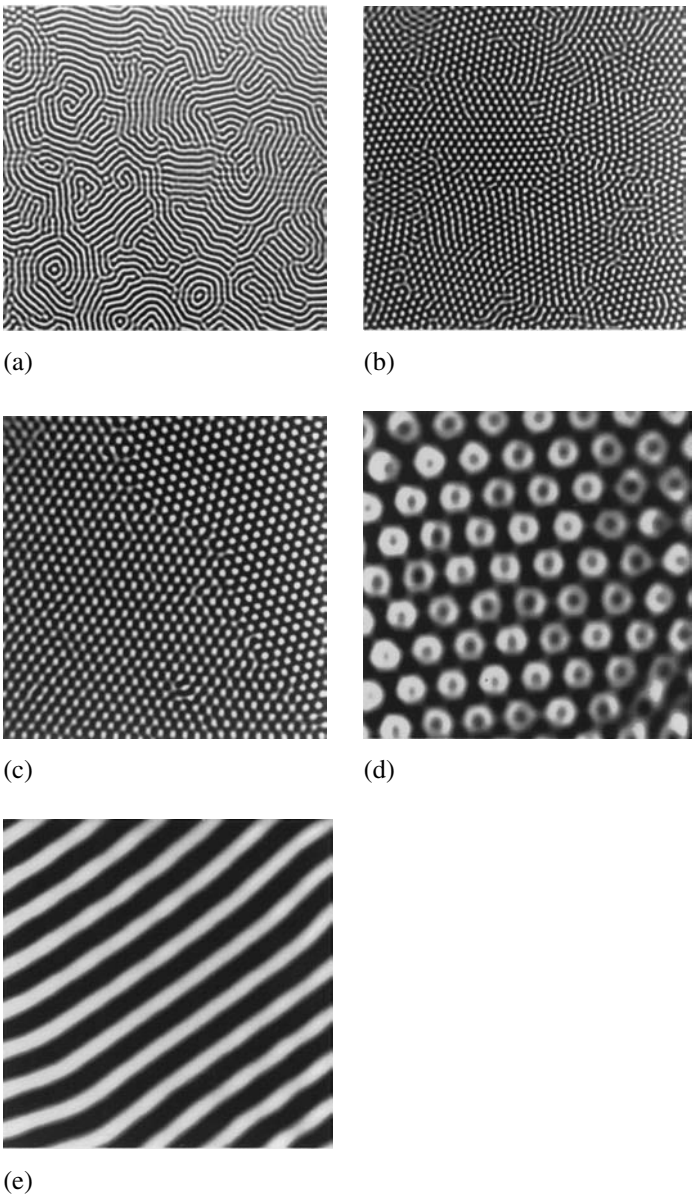

Figure 2.11. Chemical patterns obtained with the reaction diffusion system with the chlorite-iodide-malonic reaction from Gunaratne et al. (1994). The domain size is 6 mm × 6 mm. (**a**) Multiple domains with stripes with wavelength 0.11 mm. (**b**) This shows multiple domains of hexagonal patterns with different orientations. Here the wavelength is 0.12 mm. (**c**) This again shows hexagonal patterns with a single boundary separating the hexagonal lattices with different orientations: the wavelength here is 0.18 mm. (**d**) This shows a fully developed complex black eye pattern: the domain size is 1.6 mm × 1.6 mm. (**e**) When the hexagonal pattern in (**d**) becomes unstable it deforms into rhombic structures and the spots line up eventually becoming the striped pattern (in a similar way to the transition patterns in Zhu and Murray 1995): the domain is again 1.6 mm × 1.6 mm. The experimental details are given in Gunaratne et al. (1994). (Photographs reproduced courtesy of Harry Swinney)

measure domain size by γ and hence take x to be in $(0, 1)$. Then (U, V) satisfy the dimensionless equations

$$\begin{aligned} &U'' + \gamma f(U, V) = 0, \quad dV'' + \gamma g(U, V) = 0, \\ &U'(0) = U'(1) = V'(0) = V'(1) = 0. \end{aligned} \tag{2.51}$$

The non-negative heterogeneity function is defined by

$$H = \int_0^1 (U'^2 + V'^2)\, dx \geq 0, \tag{2.52}$$

which depends only on the parameters of the system and the domain scale γ. H is an 'energy function.' If we now integrate by parts, using the zero flux boundary conditions in (2.51),

$$H = -\int_0^1 (UU'' + VV'')\, dx$$

which, on using (2.51) for U'' and V'', becomes

$$H = \frac{\gamma}{d} \int_0^1 [dUf(U, V) + Vg(U, V)]\, dx. \tag{2.53}$$

If there is no spatial patterning, U and V are simply the uniform steady state solutions of $f(U, V) = g(U, V) = 0$ and so $H = 0$, as also follows, of course, from the definition (2.52).

From (2.53) we see how the scale parameter and diffusion coefficient ratio appear in the definition of heterogeneity. For example, suppose the domain is such that it sustains a single wave for $\gamma = \gamma_1$, in dimensional terms a domain length $L = L_1$ say. If we then double the domain size to $2L_1$ we can fit in two waves and so, intuitively from (2.52), H must increase as there is more heterogeneity. Since $\gamma \propto L^2$, H from (2.53) is simply quadrupled. From an embryological point of view, for example, this means that as the embryo grows we expect more and more structure. An example of this increase in structure in a growing domain is illustrated in Figure 2.18 below. Berding (1987) discusses particular applications and compares specific reaction diffusion mechanisms as regards their potential for heterogeneity.

2.5 Dispersion Relation, Turing Space, Scale and Geometry Effects in Pattern Formation Models

We first note some general properties about the dispersion relation and then exploit it further with the specific case we analysed in the last section. The formation of spatial patterns by any morphogenetic model is principally a nonlinear phenomenon. However, as we noted, a good indication of the patterns in one dimension can be obtained by a simple linear analysis. For spatial patterns to form, we saw that two conditions must